

# Stochastic Bouncy Particle Sampler

Ari Pakman\* Dar Gilboa\* David Carlson Liam Paninski

Columbia University

March 27, 2022

## Abstract

We introduce a novel stochastic version of the non-reversible, rejection-free Bouncy Particle Sampler (BPS), a Markov process whose sample trajectories are piecewise linear. The algorithm is based on simulating first arrival times in a doubly stochastic Poisson process using the thinning method, and allows efficient sampling of Bayesian posteriors in big datasets. We prove that in the BPS no bias is introduced by noisy evaluations of the log-likelihood gradient. On the other hand, we argue that efficiency considerations favor a small, controllable bias in the construction of the thinning proposals, in exchange for faster mixing. We introduce a simple regression-based proposal intensity for the thinning method that controls this trade-off. We illustrate the algorithm in several examples in which it outperforms both unbiased, but slowly mixing stochastic versions of BPS, as well as biased stochastic gradient-based samplers.

## 1 Introduction

The advent of the Big Data era presents special challenges to practitioners of Bayesian modeling because typical sampling-based learning methods have a computational cost per sample linear in the size of the dataset. This computational burden has been addressed in recent years through two major approaches (see [1] for a recent overview): (i) split the data into batches and combine posterior samples obtained in parallel from each batch, or (ii) use stochastic variants of the Markov Chain Monte Carlo (MCMC) algorithm that only query a subset of the data at every iteration. Our interest in the paper is in the latter approach, where many methods are based on modifying both steps of the Metropolis-Hastings (MH) algorithm: in the proposal step, only a mini-batch of the data is used, and the accept-reject step is either ignored or approximated [2, 3]. This strategy has been explored using proposals from Langevin [4], Riemannian Langevin [5], Hamiltonian [6] and Riemannian Hamiltonian [7] dynamics. Other relevant works include [8, 9].

Despite the success of the above approach, the absence of a (full) accept-reject step is a source of bias, whose precise size is difficult to control, and which tends to be amplified by the noisy evaluation of the gradient. Unbiased stochastic samplers are more difficult to come by. Two prominent examples are the Firefly MCMC algorithm [10], and the debiased pseudolikelihood approach of [11].

The present work is motivated by the idea that the bias could be reduced by starting from a rejection-free MCMC algorithm, avoiding thus the Metropolis-Hastings algorithm altogether. Two similar algorithms of this type have been recently proposed: the Bouncy Particle Sampler (BPS) [12, 13], and Zig-Zag Monte Carlo [14, 15]. These algorithms sample the target space through non-reversible, piecewise linear Markov processes. Non-reversibility (i.e., the failure to satisfy detailed balance) has been shown in many cases to yield faster mixing rates [16, 17, 13], while the piecewise linear nature of the sample path facilitates partially analytical computation of sample means [18].

---

\*Equal contribution.

Our contributions in this paper are twofold. On the one hand, we show that the BPS algorithm is particularly well suited to sample from posterior distributions of big datasets, because the target distribution is invariant under zero-mean noisy perturbations, such as those introduced by using mini-batches of the full dataset when evaluating the gradient of the log-likelihood. On the other hand, we argue that stochastic variants of BPS or Zig-Zag that preserve exactly the target distribution, such as the Local BPS algorithm introduced in [13] or the ZZ-SS algorithm [15], are based on overly conservative bounds (which moreover must be derived on a case-by-case basis, and in many cases may not hold at all) and therefore lead to extremely slow mixing. This leads us to propose the Stochastic Bouncy Particle Sampler (SBPS), a stochastic version of the BPS algorithm, which trades a small amount of bias for quite significantly reduced variance, yielding superior performance (and requiring no parameter tuning or derivation of problem-specific bounds) compared to existing stochastic subsampling-based Monte Carlo methods. SBPS inherits the piecewise linear sample paths of BPS, and therefore enjoys faster convergence of empirical means, particularly of rapidly varying test functions, compared to more standard approaches.

We organize this paper as follows. In Section 2 we review the Bouncy Particle Sampler; in Section 3 we study the invariance of the target distribution under noise perturbations to the BPS updates; in Section 4 we introduce SBPS; in Section 5 we discuss related works; and in Section 6 we illustrate the advantages of SBPS in several examples.

## 2 The Bouncy Particle Sampler

Consider a probability distribution

$$p(\mathbf{w}) \propto e^{-U(\mathbf{w})} \quad \mathbf{w} \in \mathbb{R}^D \quad (1)$$

where the proportionality constant is a normalization factor that may be intractable. The Bouncy Particle Sampler (BPS), proposed in [12] and formalized and developed in [13], introduces a random velocity vector  $\mathbf{v}$  distributed uniformly in the unit sphere  $S^{D-1}$ , and defines a continuous Markov process in  $(\mathbf{w}, \mathbf{v})$ . To describe this process we begin in discrete time and then take limits to obtain the continuous-time process. Denoting time by  $t$ , consider a discrete-time Markov process that acts on the variables  $(\mathbf{w}, \mathbf{v})$  as

$$(\mathbf{w}, \mathbf{v})_{t+\Delta t} = \begin{cases} (\mathbf{w} + \mathbf{v}\Delta t, \mathbf{v}) & \text{with probability } 1 - \Delta t[G]_+ \\ (\mathbf{w} + \mathbf{v}\Delta t, \mathbf{v}_r) & \text{with probability } \Delta t[G]_+ \end{cases} \quad (2)$$

---

**Algorithm 1** Bouncy Particle Sampler

---

```

Initialize particle position  $\mathbf{w}_0 \in \mathbb{R}^D$  and velocity  $\mathbf{v} \in S^{D-1}$ 
while desired do
  Sample first arrival  $t_b$  from Poisson process with rate  $\lambda(t) = [\mathbf{v} \cdot \nabla U(\mathbf{w}_0 + \mathbf{v}t)]_+$ 
  Sample first arrival  $t_r$  from Poisson process with constant rate  $\lambda_r$ 
  Let  $t = \min(t_b, t_r)$ 
  Move  $\mathbf{w}_t = \mathbf{w}_0 + \mathbf{v}t$ ,
  if  $t_b < t_r$  then
    Reflect velocity according to  $\mathbf{v} \leftarrow \mathbf{v} - 2 \frac{(\mathbf{v} \cdot \nabla U(\mathbf{w}_t)) \nabla U(\mathbf{w}_t)}{\|\nabla U(\mathbf{w}_t)\|^2}$ 
  else
    Refresh: sample velocity  $\mathbf{v} \sim \text{Unif}[S^{D-1}]$ 
  end if
  Let  $\mathbf{w}_0 \leftarrow \mathbf{w}_t$ 
end while
return Return piecewise linear trajectory of  $\mathbf{w}$ 

```

---

where

$$[x]_+ = \max(x, 0), \quad (3)$$

$$G = \mathbf{v} \cdot \nabla U(\mathbf{w}), \quad (4)$$

and

$$\mathbf{v}_r = \mathbf{v} - 2 \frac{(\mathbf{v} \cdot \nabla U(\mathbf{w})) \nabla U(\mathbf{w})}{\|\nabla U(\mathbf{w})\|^2}. \quad (5)$$

Note that  $G$  in (4) is the directional derivative of  $U(\mathbf{w})$  in the direction  $\mathbf{v}$ , and  $\mathbf{v}_r$  is a reflection of  $\mathbf{v}$  with respect to the plane perpendicular to the gradient  $\nabla U$ , satisfying  $\mathbf{v}_r \cdot \nabla U = -\mathbf{v} \cdot \nabla U$  and  $(\mathbf{v}_r)_r = \mathbf{v}$ . In other words, the particle  $\mathbf{w}$  moves along a straight line in the direction of  $\mathbf{v}$  and this direction is reflected as (5) with probability  $\Delta t[G]_+$ . This probability is non-zero only if the particle is moving in a direction of lower target probability  $p(\mathbf{w})$ , or equivalently higher potential  $U(\mathbf{w})$ .

Applying the transition (2) repeatedly and taking  $\Delta t \rightarrow 0$ , the random reflection point becomes an event in an inhomogeneous Poisson process with intensity  $[G]_+$ . The resulting sampling procedure generates a piecewise linear Markov process [19], and is summarized in Algorithm 1. Note that the algorithm also includes occasional resamplings of  $\mathbf{v}$ , to ensure ergodicity [13]. Remarkably, in the limit  $\Delta t \rightarrow 0$ , the algorithm leaves the joint factorized distribution  $p(\mathbf{w})p(\mathbf{v})$  invariant [13], as we review in Section A.1.

The Zig-Zag process, proposed in [14, 15], is similar to BPS, but each component of the velocity can take only  $+1$  or  $-1$  values, and the piecewise linear trajectories change direction only in a *single* coordinate at each random breakpoint.

### 3 Noise Resilience

Let us consider a case in which only a noisy version of the gradient is available to evaluate the probability of bouncing in (2) and to compute the reflected velocity in (5). In the Big Data scenario described in the next section, the noise is the result of using a random subset of the full data set at each evaluation of the gradient. Such a noisy gradient can be represented as

$$\nabla \tilde{U}(\mathbf{w}) = \nabla U(\mathbf{w}) + \mathbf{n}_w, \quad \mathbf{n}_w \sim p(\mathbf{n}_w | \mathbf{w}), \quad \mathbf{n}_w \in \mathbb{R}^D \quad (6)$$

where  $p(\mathbf{n}_w | \mathbf{w})$  has zero mean.

**Theorem:** *The invariance of  $p(\mathbf{w})p(\mathbf{v})$  under the BPS algorithm is not affected by a zero-mean noise perturbation (6) if  $\mathbf{n}_{w_1}$  and  $\mathbf{n}_{w_2}$  are independent for  $\mathbf{w}_1 \neq \mathbf{w}_2$ .*

See Section A.2 for the proof. Defining  $\tilde{G} = \mathbf{v} \cdot \nabla \tilde{U}(\mathbf{w})$ , the intensity of the inhomogeneous Poisson process  $[\tilde{G}]_+$ , which determines the time of the velocity bounce, now becomes stochastic, and the resulting point process is called a doubly stochastic, or Cox, process [20, 21]. The effect of the gradient noise is to increase the average point process intensity, since  $\langle [\tilde{G}]_+ \rangle \geq \langle [\tilde{G}]_+ \rangle$ , from Jensen's inequality. This leads to more frequent bounces and typically a slower mixing of the Markov process, as illustrated in Figure 1.

Many Cox processes in the literature are based on Poisson intensities obeying stochastic differential equations, or assume that the joint distribution at several  $\mathbf{w}$ 's has a non-trivial  $\mathbf{w}$ -dependent structure. Our case is different because we assume that  $\mathbf{n}_{w_1}$  and  $\mathbf{n}_{w_2}$  are independent even when  $\mathbf{w}_1$  and  $\mathbf{w}_2$  are infinitesimally close. We can generate samples under such a noisy intensity using the thinning method [22], a rejection sampling approach which only requires realizations from the noisy intensity at a finite set of points (discussed at more length in the next section). The one technical challenge with this approach is that to ensure correctness of the algorithm we must guarantee that the proposal intensity is greater than the noisy intensity  $[\mathbf{v} \cdot \nabla \tilde{U}(\mathbf{w})]_+$  with probability one; in most cases this is not possible, but nonetheless we find empirically that useful approximate bounds can be constructed which hold with sufficiently high probability to lead to good approximate samplers.

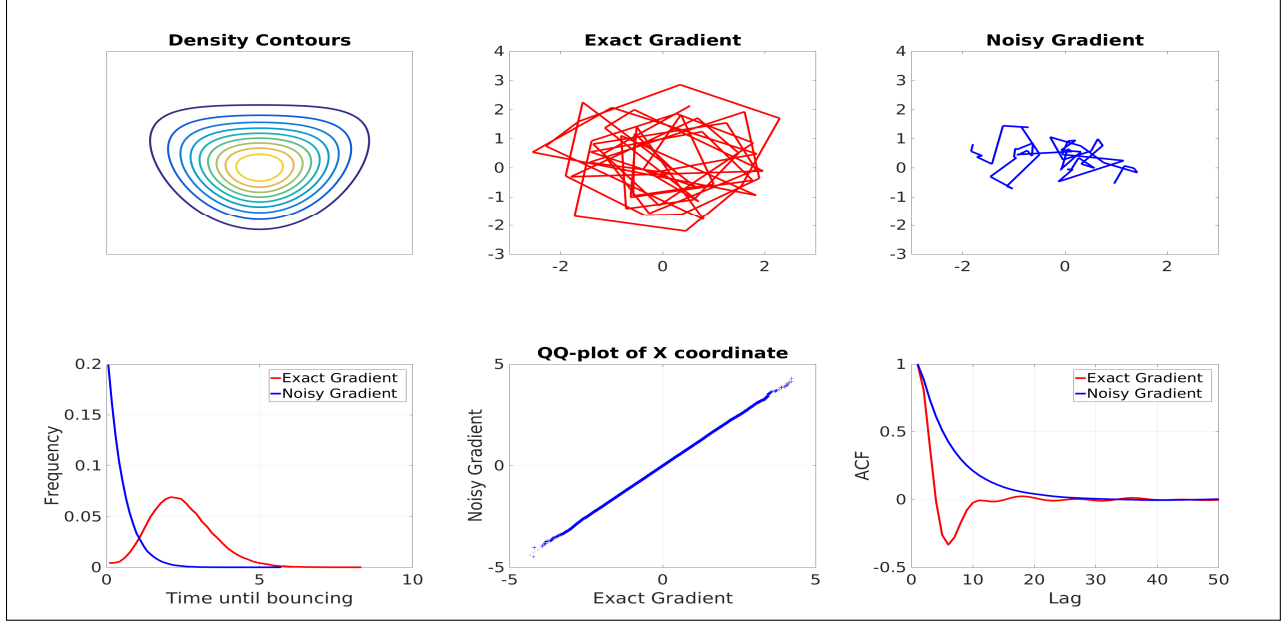


Figure 1: *Above*: Contour plot of the 2D density considered and sample BPS trajectories during 50 bounces, with exact and noisy gradients. The noise was sampled in each component from a  $\mathcal{N}(0, 5^2)$  distribution. *Below, Left*: smoothed histogram of travel times until bouncing, with shorter times for noisy gradients. *Middle*: QQ-plot of one of the coordinates, showing that the invariant distribution is not changed by the noise. *Right*: ACFs of one of the coordinates, with slower mixing per iteration in the noisy case. However, note that these ACF plots do not account for computational cost per iteration; see Appendix E.1 for further discussion.

## 4 Sampling from Big Data posteriors

In a prototypical Bayesian setting, we have a prior  $f(\mathbf{w})$ , i.i.d. data points  $x_i$ , and the negative log-posterior gradient is

$$\nabla U(\mathbf{w}) = -\nabla \left[ \log f(\mathbf{w}) + \sum_{i=1}^N \log p(x_i|\mathbf{w}) \right]. \quad (7)$$

When  $N$  is big we consider replacing the above gradient by the noisy approximation

$$\nabla \tilde{U}(\mathbf{w}) = -\nabla \left[ \log f(\mathbf{w}) + \frac{N}{n} \sum_{i=1}^n \log p(x_{r_i}|\mathbf{w}) \right], \quad (8)$$

where  $n \ll N$  and the  $n$  indices  $\{r_i\}$  are sampled randomly without replacement. To sample from the posterior using the noisy gradient (8), we want to simulate the first arrival time in a doubly stochastic Poisson process with random intensity  $[\tilde{G}(t)]_+$ , where

$$\tilde{G}(t) = \mathbf{v} \cdot \nabla \tilde{U}(\mathbf{w} + \mathbf{v}t). \quad (9)$$

Note that in the above expression  $\tilde{U}$  is a stochastic process, and for each  $t$  it requires a different mini-batch sample. The thinning method [22] is a form of rejection sampling which consists in proposing a first arrival time  $t$ , sampled from an inhomogeneous Poisson process with intensity  $\lambda(t)$  such that

$$\lambda(t) \geq [\tilde{G}(t)]_+. \quad (10)$$

The particle moves a distance  $t\mathbf{v}$ , and accepts the proposal to bounce the velocity with probability  $[\tilde{G}(t)]_+/\lambda(t)$ . Note that this accept-reject step is different from the MH algorithm [23], since the particle always moves the

distance  $t\mathbf{v}$ , and a rejection only affects the velocity bouncing. This can greatly improve the efficiency of the sampler. As in the noiseless case, one should in general also resample  $\mathbf{v}$  occasionally, to ensure ergodicity [13], although in the examples we considered we found that these velocity refreshes were not empirically necessary, since the mini-batch noise serves to randomize the velocity sufficiently, preventing “non-ergodic” trajectories that do not explore the full space.

In some special cases one can derive a bound  $\lambda(t)$  in (10) that always holds [13]. But this is atypical, due to the dependence of  $\tilde{G}(t)$  in (9) on the changing velocity  $\mathbf{v}$  and the mini-batch noise. Even when such bounds do exist, they tend to be conservatively high, leading to an inefficient sampler with many rejected proposals (wasting many mini-batches of data) before accepting.

Instead, we propose below an adaptive approximate bound which achieves a bias-variance trade-off between the frequency of the bounce proposals and a controllable probability of bound violation, i.e.,  $[\tilde{G}(t)]_+/\lambda(t) > 1$ .

## 4.1 Proposal Intensity from Local Regression

Our approach to an adaptive and tractable proposal intensity  $\lambda(t)$  relies on a predictive model of  $\tilde{G}$  based on previous observations; the key idea is that nearby  $\tilde{G}$  values are in general correlated, and we can exploit these correlations to obtain better proposals. The upper value of the resulting predictive confidence band can then be used as  $\lambda(t)$ , and this band is adaptively updated as more proposals are generated.

While there are many possibilities for such a predictive model, we found that a simple local linear model was very effective and computationally trivial. Consider then the linear regression of  $m$  observed values  $\tilde{G}_i \equiv \tilde{G}(t_i)$  since the previous bounce,

$$\tilde{G}_i = \beta_1 t_i + \beta_0 + \varepsilon_{t_i} \quad \varepsilon_{t_i} \sim N(0, c_{t_i}^2) \quad i = 1, \dots, m, \quad (11)$$

where the noise variance can be estimated from the mini-batch in (8) as

$$c_t^2 = \frac{N^2}{n} \left(1 - \frac{n}{N}\right) \text{Var}_i [\mathbf{v} \cdot \nabla \log p(x_{r_i} | \mathbf{w})]. \quad (12)$$

Here  $\text{Var}_i$  denotes the sample variance of the mini-batch, and we included the *finite population correction factor*  $(1 - \frac{n}{N})$  that takes into account that the indices  $\{r_i\}$  are sampled without replacement. The Gaussian assumption on the noise of  $\tilde{G}(t)$  in (11) is valid when the mini-batch is sufficiently large that we can appeal to a central limit theorem argument. (For very heavy-tailed mini-batch noise we could consider more robust estimators, but we do not pursue this direction here.)

Adding a Gaussian prior to  $\beta_1$ , and defining  $\mathbf{x}_i \equiv (1, t_i)$ , the log posterior of  $\boldsymbol{\beta} = (\beta_0, \beta_1)^T$  is

$$2 \log(p(\boldsymbol{\beta} | \{t_i, \tilde{G}_i, c_{t_i}^2\})) = -\sum_{i=1}^m \frac{(\tilde{G}_i - \mathbf{x}_i \cdot \boldsymbol{\beta})^2}{c_{t_i}^2} + \frac{(\beta_1 - \mu)^2}{\sigma^2} + \text{const.} \quad (13)$$

Let  $\hat{\boldsymbol{\beta}}$  and  $\boldsymbol{\Sigma}$  be the mean and covariance of this distribution. Using these estimates, we obtain the predictive distribution  $\hat{G}(t)$  for  $\tilde{G}(t)$  for  $t > t_m$ ,

$$\hat{G}(t) = \hat{\beta}_1 t + \hat{\beta}_0 + \eta_t \quad \eta_t \sim N(0, \rho^2(t)) \quad (14)$$

where

$$\rho^2(t) = \mathbf{x} \boldsymbol{\Sigma} \mathbf{x}^T + c_{t_m}^2 \quad (15)$$

with  $\mathbf{x} = (1, t)$ . Note that as usual the noise variance is different in (11) and (14), since in (11) we are fitting observed pairs  $\tilde{G}_i, t_i$ , while in (14) we are predicting the value of  $\tilde{G}(t)$  and we include the uncertainty from the  $\hat{\boldsymbol{\beta}}$  estimates. Also, for simplicity we extrapolate the observation noise to be the same as in the last mini-batch,  $c_{t_m}^2$ .

We can now construct a tractable approximate thinning proposal intensity by choosing a constant predictive confidence band multiple  $k$ , and defining  $\gamma(t)$  as a linear interpolation between selected points along the curve

$$\hat{\beta}_1 t + \hat{\beta}_0 + k\rho(t). \quad (16)$$

(We discuss the choice of  $k$  in more depth below.) The proposal intensity is now

$$\lambda(t) = [\gamma(t)]_+, \quad (17)$$

and since  $\lambda(t)$  is piecewise linear, sampling from an inhomogeneous Poisson process with rate  $\lambda(t)$  can be done analytically by solving a quadratic equation using the inverse CDF method. When a bounce time is proposed at time  $t$ , the particle moves a distance  $t\mathbf{v}$ , a noisy observation  $\tilde{G}(t)$  is made as in (9) and the bounce time is accepted with probability  $[\tilde{G}(t)]_+/\lambda(t)$ . If the bounce proposal is accepted, the velocity is reflected as in (5) (using  $\tilde{U}$  instead of  $U$ ), and the set of observed values is reinitialized with  $(-\tilde{G}(t), c_t)$ , which are the values one would obtain from sampling the same mini-batch *after* the bounce, since  $\mathbf{v}_r \cdot \tilde{U} = -\mathbf{v} \cdot \tilde{U} = -\tilde{G}(t)$ . On the other hand, if the proposal is rejected, the observed  $(\tilde{G}(t), c_t)$  are added to the set of observed values. The hyperparameters  $\mu, \sigma^2$  of the regression model for  $\beta_1$  can be learned by performing, after each bounce, a stochastic gradient ascent step on the marginal likelihood,  $p(\{\tilde{G}_i\}|\mu, \sigma^2)$ ; this gradient can be computed analytically and therefore does not significantly impact the computational cost.

The constant  $k$  in (16) controls the tradeoff between bias from possible  $[\tilde{G}(t)]_+/\lambda(t) > 1$  cases and lower computational cost: higher  $k$  leads to a more conservative (higher) proposal intensity and therefore a less-biased but more data-inefficient sampler. We explore this tradeoff more systematically in Appendix E.

The linear model for  $\tilde{G}$  is good when the target distribution can be locally approximated by a Gaussian, since  $\tilde{G}(t)$  in (9) is a projection of the derivative of the negative log posterior. When the posterior is highly non-Gaussian, this approach can be easily generalized by using a decaying weight for more-distant observations, leading to a local regression; the scale of this decay can be fit again via stochastic gradient ascent on the predictive likelihood. We have also explored a Gaussian Process regression model, but did not find that it improved over the linear model in the cases we considered. In any case it is important to track as a bias diagnostic the rate at which the bound is violated, i.e., cases with  $[\tilde{G}(t)]_+/\lambda(t) > 1$ ; if this rate is significantly higher than expected under the local linear regression model, then a different approach should be considered.

Finally, note that the directional derivative of  $\tilde{U}(\mathbf{w})$  needed in (9) can in many cases be computed at a cheaper cost (by a factor of  $d = \dim(\mathbf{w})$ ) than the full gradient. The latter is only needed when a bounce is accepted. This is in contrast to other gradient based samplers which require the full gradient at every step.

We dub this approach to BPS with noisy gradients Stochastic BPS (SBPS). See appendix B for pseudocode. Figure 2 illustrates the evolution of these dynamic proposal intensities in a simple example. In Appendix C, we consider a variant to SBPS, called pSBPS, that includes learning a diagonal preconditioning factor for the gradient, and leads to a more efficient exploration of the space when the posterior is highly anisotropic and roughly axis-aligned.

## 5 Related Works

Having introduced the SBPS, we now pause to examine its relation with previous works on stochastic MCMC samplers.

**Biased Samplers:** Many stochastic gradient MCMC samplers (e.g. [4, 5, 6]) can be formulated exactly in terms of continuous stochastic dynamics with a Wiener process [7], but they lead to biased samplers because (i) the Gaussian assumption in the noise may not hold for small mini-batches, and (ii) the MH correction to the time discretization is avoided or approximated. Recently, irreversible samplers have been studied in this context [24]. Choosing the step size in these samplers can be quite challenging, as discussed below: too-large step sizes lead to high levels of bias on the estimated posterior, while too-small step sizes lead to very slow mixing, and in generic high-dimensional examples there is no way to automatically tune the step

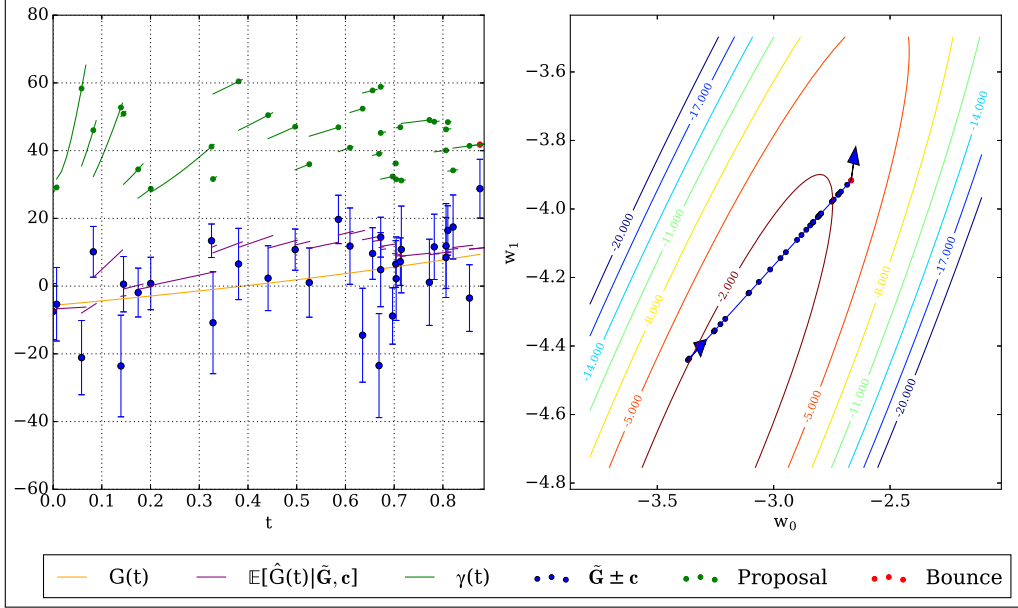


Figure 2: Thinning proposal intensity for bounce times from a linear regression predictive confidence interval applied to a two-dimensional logistic regression posterior with  $N = 1000, n = 100$ . *Left:* Starting from  $t = 0$ , the piecewise linear  $\gamma(t)$  defined in eq (16) is used to propose bounce times (green points). As these proposals are rejected additional observations  $\tilde{G}_i$  are made until a proposal is accepted (red point). The decrease in the slope of the proposal intensities indicates the decreasing uncertainty in the estimation of the regression parameters as the number of observations increases; note that the linear approximation for the true  $G(t)$  is quite accurate here. Note also the reduced observation frequency at lower values of  $G(t)$  indicating more efficient sampling than is achievable with the bounds used in [13, 15], which are much higher (more conservative) and constant along a trajectory and thus lead to a uniform proposal rate. These bounds as well as the bound used for the lipSBPS algorithm described in 6.1 were concentrated in the range  $[10^4, 2 * 10^4]$  for this data. *Right:* The corresponding SBPS particle trajectory, with arrows indicating the initial velocity and the velocity after the bounce. The contours show the Laplace approximation of the (unnormalized) log posterior.

size (though see [25] for recent progress on this important issue). In contrast, the bias in SBPS, controlled by the constant  $k$ , does not come from discretizing the continuous time dynamics, but from violations of the thinning bound when  $[\tilde{G}(t)]_+/\lambda(t) > 1$ , and as discussed above, this bound violation rate is quite easy to track.

**Exact non-BPS-like Samplers:** The Firefly MCMC algorithm [10] yields unbiased samples while only querying a subset of data points at each MCMC iteration. It is an elegant method based on augmenting the target distribution with binary variables associated to each data point, but its drawbacks are (i) the need to compute tight lower bounds on the likelihood function, which depend on the particular distribution of interest and require a sweep through all the data, (ii) mixing can be extremely slow, as shown in some simple examples in [26, 1], and (iii) all the dataset must be available for access all the time. In contrast, the SBPS has excellent mixing speed (see next Section), can be implemented while accessing fresh mini-batches at every proposal, and our simple Bayesian linear regression proposal applies to generic smooth distributions, with no need to rederive new bounds with each new target density.

Another recent novel proposal is the work [11], based on debiased pseudolikelihood combined with variance reduction techniques. This method is relatively more complex, and we have not yet systematically compared it against SBPS.

**Exact BPS-like Samplers:** Two subsampling variants of BPS which preserve the exact distribution have been recently proposed. The work [13] presents a stochastic variant of the basic BPS algorithm, called Local BPS, that needs a pre-processing step of computational cost  $O(N \log N)$ . The work [15] proves a noise invariance result for the Zig-Zag process [14], similar in spirit to our results for BPS, and proposes a stochastic algorithm called ZZ-SS. These approaches have three major disadvantages. First, both Local BPS and ZZ-SS use only one data point in each iteration, while SBPS can be applied to mini-batches of arbitrary size  $n$ , as long as the CLT holds; as discussed below,  $n \approx 10^2$  led to very good performance in our simulations. Modern processors can easily parallelize the gradient computations over the mini-batch points, making it about as fast to process a mini-batch of size  $n \approx 10^2$  as of size  $n = 1$ ; this leads to a two-order-of-magnitude speedup for SBPS. Secondly, the requirement to preserve the distribution exactly in Local BPS and ZZ-SS leads to extremely conservative thinning bounds, which in turn yield a very slow exploration of the space (as a function of the number of datapoints observed), as we will see below. Finally, these bounds need to be rederived for each new model (and in many models may not hold at all), unlike SBPS which is a generic algorithm that can be used for any smooth posterior distribution.

## 6 Experiments

### 6.1 Logistic Regression

Although simpler MCMC methods perform well in Bayesian logistic regression (BLR) models [27], we begin with a simple BLR example as a well-understood test case for running careful comparisons of SBPS against a few of the existing stochastic MCMC methods discussed in the previous section. To generate the data, we drew the components of the true parameters  $\mathbf{w} \in \mathbb{R}^d$  from a uniform distribution in  $[-5, 5]$  and  $N$  data points  $\{\mathbf{x}_i\}$  from a  $d$ -dimensional zero-mean multivariate Gaussian, with one component of the diagonal covariance set to 6 and all the rest to 1, resulting in an anisotropic posterior. Labels  $\{y_i\}$  are drawn from

$$y_i \sim \text{Bern}(\sigma(\mathbf{w} \cdot \mathbf{x}_i)) \quad (18)$$

where  $\sigma(x) = 1/(1 + e^x)$ . In the regime  $d \ll N$  the Laplace approximation holds fairly well, providing another good comparison method. Figure 3 shows results for this model with  $N = 1000$ ,  $d = 20$ . The SBPS predictive confidence interval multiplier was  $k = 3$  and the mini-batch size  $n = 100$ .

We run comparisons against the biased stochastic samplers Stochastic Gradient Langevin Dynamics (SGLD) [4] and multivariate Stochastic Gradient Nose-Hoover Thermostat (mSGNHT) [28] with fixed step sizes. As noted above, choosing optimal step sizes for these samplers is challenging. In this case, to allow SGLD and mSGNHT to achieve their best possible performance, we performed a scan to find the largest (fastest-mixing) step size that did not lead to overly large bias compared to the Laplace approximation. (Note, importantly, that this scan is expensive and is not possible in high-dimensional examples where the Laplace approximation does not hold - i.e., precisely the cases where MCMC methods are most valuable.) See Appendix D for full details of this scan, which led to an optimal step size of 0.1 for SGLD. Larger step sizes led to visible biases in the sampled posterior (data not shown); we also show the results with step size 0.01 for comparison to note that the results do depend sensitively on this parameter.

We also compare against Zig-Zag with sub-sampling (ZZ-SS) [15]. In our hands Local BPS [13] was slow, unstable, and challenging to debug, so instead we ran comparisons against an unbiased method we call lipSBPS (short for Lipshitz BPS), where the velocity bounces occur as first arrival events in a Poisson process with noisy intensity  $[\mathbf{v} \cdot \nabla \tilde{U}(\mathbf{w})]_+$  built from a noisy gradient (8) of minimal size  $n = 1$ , and simulated with thinning using an *exact* upper bound derived in Appendix F. One can easily verify that the resulting stochastic process on  $(\mathbf{w}, \mathbf{v})$  is identical to that of Local BPS. Our bound is higher than that used in [13] by up to a factor of 2, which results in up to twice more bounce proposals. On the other hand, our bound can be computed in  $O(N)$ , does not require non-negative covariates and can be used also for  $n > 1$ . Again, we note that this lipSBPS method, like Local BPS and ZZ-SS, are not generally applicable because the derived bounds only apply in special cases.

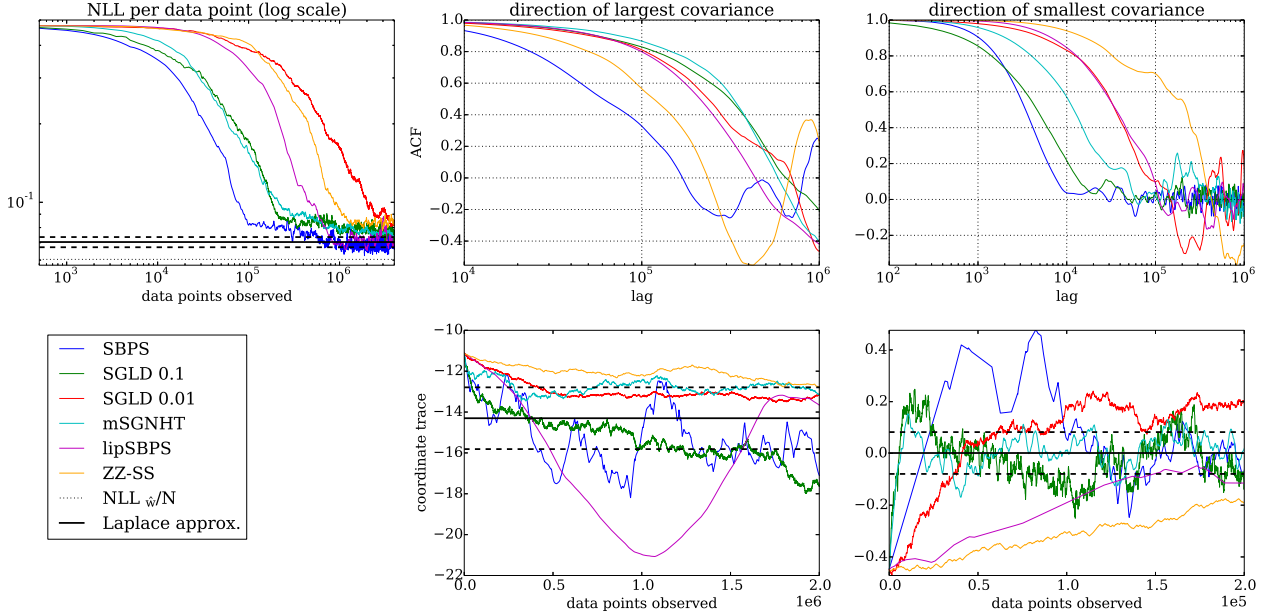


Figure 3: Logistic regression posterior sampling, with  $d = 20$ ,  $N = 1000$ ,  $k = 3$ ,  $n = 100$  (best seen in color). *Top Left:* Negative Log Likelihood (NLL) per data point of samples from SBPS compared with SGLD (with step sizes 0.01, 0.1) [4], mSGNHT [28] with step size 0.1, lipSBPS (defined in the text) and SS-ZZ [15]. All the samplers were initialized at the same random positions. Also shown are the normalized NLL of the MAP estimator  $NLL_{\hat{w}}/N$  and the mean  $\pm$  standard deviation NLL of the Laplace approximation (distributed according to  $\frac{1}{2N}\chi^2(d) + NLL_{\hat{w}}/N$ ). The continuous samplers (SBPS, SS-ZZ, lipSBPS) were run to match the data cost of the discrete samplers (SGLD, mSGNHT), and their ACFs were computed by discretizing the continuous paths uniformly to obtain the same number of samples. The CPU runtime for this sampling was 35 times higher for the  $n = 1$  SS-ZZ and lipSBPS, than for the  $n = 100$  SBPS. The runtime of the latter was 2.5 times higher than SGLD and mSGNHT. *Center/Right:* Trajectories and ACFs in the directions of largest and smallest posterior covariance (largest and smallest eigenvalues of the Laplace approximation inverse Hessian). The ACFs were calculated after discarding burn-in, while the trajectory plots only show initial convergence.

See Figure 3 for a summary of the results. We find that SBPS outperforms the optimally tuned SGLD and mSGNHT. Convergence of SBPS was orders of magnitude faster than lipSBPS and ZZ-SS. While the latter two methods are unbiased, our results suggest that the small bias introduced by the approximate SBPS thinning proposal intensity is worth the massive reduction in variance that the method provides.

In Appendix E we explore the effects of the SBPS hyperparameters:  $k$ ,  $n$ , and the rate at which velocity refreshes are performed. The conclusion is that in this logistic example no manual hyperparameter tuning was required (in stark contrast to the careful step size tuning required for SGLD): the bias-controlling constant  $k$  can be set in the range  $k \in [3, 5]$  (consistent with the tails of the Gaussian residual distribution in the linear regression model) and the mini-batch size  $n$  should be small, but large enough that the CLT holds approximately to justify the noise term in (11);  $n = 100$  worked well, but the results were not sensitively dependent on  $n$ . For small values of  $n$  the mini-batch variability provided sufficient velocity randomness that no additional velocity refreshes were necessary, so we did not have to tune this refresh-rate parameter either.

## 6.2 2D Highly non-Gaussian Posterior

Next we explored a case where simple Laplace approximations no longer suffice. Figure 4 shows results for a highly non-log-concave, anisotropic 2D ring-shaped distribution squashed along one axis. This target density

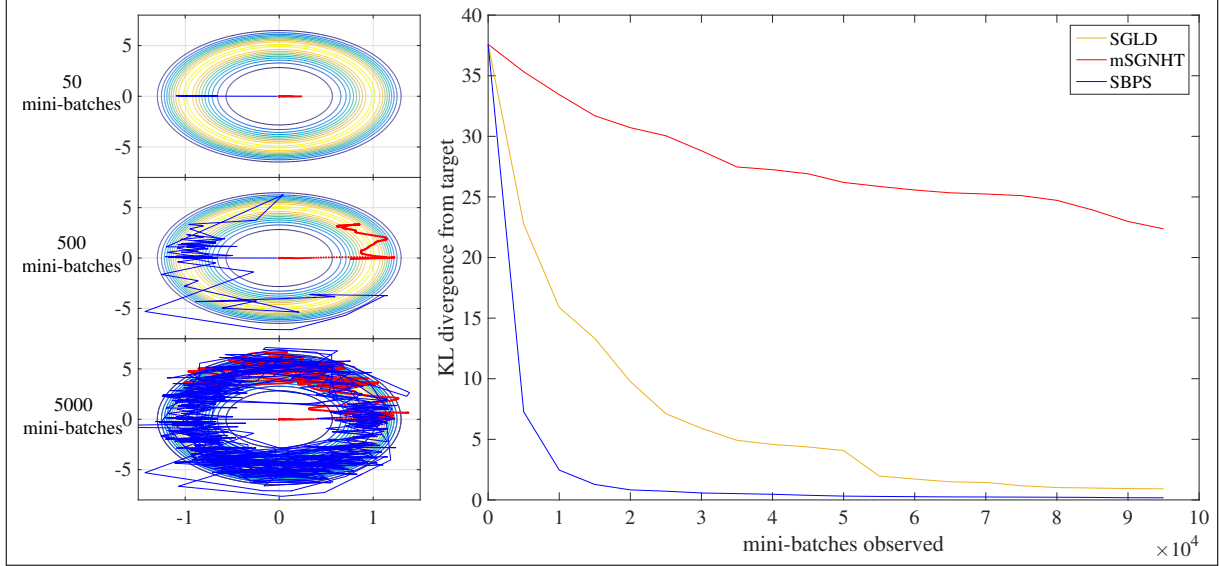


Figure 4: Sample traces and KL divergence as a function of the amount of data observed for different stochastic samplers on a ring-shaped 2D target, based on an average of 5 runs with  $n = 10, N = 1000, k = 5$ , generated as described in Section 6.2. SBPS mixes significantly faster than the other two methods.

was formed by taking the product of  $N = 1000$  densities proportional to  $\exp\left(-\frac{[((w_1-f)/a)^2+((w_2-e)/b)^2-c^2]^2}{2d}\right)$  with  $[a, b, c, d, e, f] \sim \mathcal{N}([1, 5, 1, 1, 0, 0], 10^{-2} * [1, 25, 1, 10^{-2}, 1, 1])$ . Figure 4 shows comparisons with SGLD and mSGNHT, while Local BPS and SS-ZZ cannot be applied since, unlike the logistic regression case, there seems to be no simple exact upper bound for thinning in this case.

The KL divergence of the sampled density from the true distribution was quantified by discretizing both the true distribution and the sampler output on a grid. Denoting the discrete target distribution  $P$  and the normalized histograms calculated from the outputs of the different samplers as  $Q_i$ , the KL divergences between  $P$  and  $Q_i$  were calculated. These calculations were repeated using subsets of the sampler outputs of increasing size, corresponding to different numbers of mini-batches of data observed.

The step sizes for SGLD and mSGNHT were chosen as the largest (fastest-mixing) step sizes that did not lead to visible biases in the sampled posterior. (Note that, similarly to the preceding logistic example, in a higher-dimensional case this visually-guided choice of step size would not be possible.) In contrast, again, minimal hyperparameter tuning was necessary for SBPS here. Nonetheless, SBPS mixing was faster by an order of magnitude than the other methods, even compared to mSGNHT, which also introduces a momentum variable analogous to the SBPS velocity.

### 6.3 Continuous Trajectory Sampling

A unique feature of the BPS/Zig-Zag samplers and their stochastic variants is that their output is a continuous trajectory instead of discrete samples. Given  $\mathbf{w}_0$  and a set of  $R$  velocities and bounce times  $\{\mathbf{v}_i, t_i\}$ , the estimated expectation of a test function  $f(\mathbf{w})$  is

$$\langle f(\mathbf{w}) \rangle_{BPS} \equiv \frac{1}{T} \sum_{i=0}^{R-1} \int_0^{t_i} f(\mathbf{w}_i + \mathbf{v}_i t) dt \quad (19)$$

where  $\mathbf{w}_{i+1} = \mathbf{w}_i + \mathbf{v}_i t_i$  and  $T$  is the total particle travel time. For simple test functions this integral is analytic, while more generally it can be computed numerically with standard efficient one-dimensional quadrature methods. When  $f(\mathbf{w})$  varies across a characteristic length  $r$  shorter than the average trajectory length  $b$

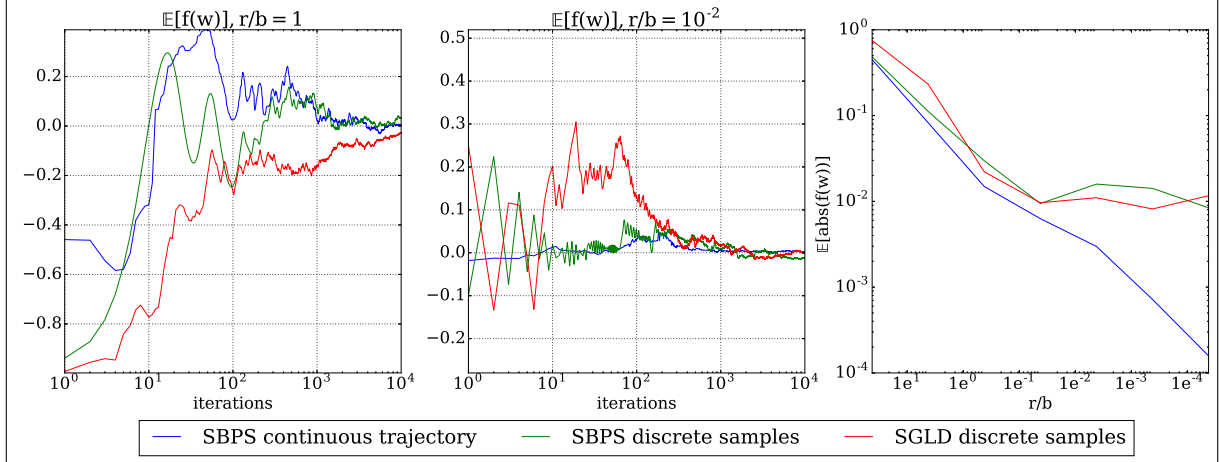


Figure 5: Estimated expectation of  $f(w) = \sin((w - \hat{w}/r)$ , with different values for the ratio  $r/b$  where  $b$  is the average linear trajectory length, under continuous and discrete samples. For this example  $b \approx 2 \times 10^{-2}$ . The posterior distribution and parameter settings are the same as in Figure 3. Assuming the Laplace approximation holds, the expectation of  $f$  is 0. *Left*: For  $r/b = 1$  there is little difference in convergence using continuous or discrete samples. *Center*: For  $r/b = 10^{-2}$  the continuous SBPS expectation converges faster than the discrete. *Right*: Expectation of the absolute value of the test function averaged over 5 runs of 1000 epochs, as a function of the ratio  $r/b$ . The advantage of the continuous expectation when this ratio is  $r/b \ll 1$  is evident.

of the linear segments, we intuitively expect the error in the estimate (19) to be smaller than in estimators based on discrete samples. Note that this advantage tends to diminish for higher SBPS noise, since the linear segments become shorter.

Figure 5 explores empirically this idea in a simple setting by comparing the value of the expectation of  $f(w) = \sin((w - \hat{w})/r)$  under the posterior distribution of the logistic example considered above. Here  $(w, \hat{w})$  are the first coordinates of the vectors  $(\mathbf{w}, \hat{\mathbf{w}})$ ,  $\hat{\mathbf{w}}$  is the MAP value of the logistic posterior, and  $r$  controls the characteristic length of  $f$ . As expected, note that the error in the expectation is lower in the continuous case for  $r/b < 1$ .

## 7 Conclusions

This paper introduced a non-reversible sampler that can be applied to big datasets by means of subsampling the data in each iteration. At the price of a small, controllable bias, it provides the benefits of (i) high mixing speed associated with non-reversibility, and (ii) continuous sample trajectories, with (iii) minimal hyperparameter tuning required, leading to state of the art performance and making it a convenient alternative to biased, difficult-to-tune MH-based stochastic samplers.

# Stochastic Bouncy Particle Sampler

## Appendix

### A Proof of Invariance under Noisy Gradients

In this section we start with a simple reformulation of the proof in [13] that the BPS Markov process leaves invariant the distribution  $p(\mathbf{w}, \mathbf{v}) = p(\mathbf{w})p(\mathbf{v})$  where

$$p(\mathbf{w}) \propto e^{-U(\mathbf{w})} \quad \mathbf{w} \in \mathbb{R}^D \quad (\text{A.1})$$

$$p(\mathbf{v}) = \text{Unif}[S^{D-1}], \quad (\text{A.2})$$

where  $S^{D-1}$  is the  $D$ -dimensional one-sphere. This will set the stage for the noisy case considered next. For a more formal and detailed treatment of the BPS algorithm, including ergodicity, see [13]. For simplicity, we do not include here the velocity refreshments, which do not change the proof.

#### A.1 Exact Gradient

To understand why the algorithm is correct, consider how the transition rule (2) acts on the probability density  $p(\mathbf{w}, \mathbf{v})$ ,

$$p_{t+\Delta t}(\mathbf{w}, \mathbf{v}) = [p_{t+\Delta t}(\mathbf{w}, \mathbf{v})]_d + [p_{t+\Delta t}(\mathbf{w}, \mathbf{v})]_r \quad (\text{A.3})$$

The two terms in (A.3) correspond to the two ways to reach  $(\mathbf{w}, \mathbf{v})$  at time  $t + \Delta t$ . First, we can start at  $(\mathbf{w} - \mathbf{v}\Delta t, \mathbf{v})$  at time  $t$  and move a distance  $\mathbf{v}\Delta t$  without bouncing. This occurs with probability  $1 - \Delta t[\mathbf{v} \cdot \nabla U]_+$ , so we have

$$[p_{t+\Delta t}(\mathbf{w}, \mathbf{v})]_d = (1 - \Delta t[\mathbf{v} \cdot \nabla U]_+)p_t(\mathbf{v})p_t(\mathbf{w} - \mathbf{v}\Delta t) \quad (\text{A.4})$$

$$= (1 - \Delta t[\mathbf{v} \cdot \nabla U]_+)p_t(\mathbf{v})(p_t(\mathbf{w}) - \Delta t\mathbf{v} \cdot \nabla p_t(\mathbf{w}) + O(\Delta t^2)) \quad (\text{A.5})$$

$$= p_t(\mathbf{v})p_t(\mathbf{w})[1 + \Delta t\mathbf{v} \cdot \nabla U - \Delta t[\mathbf{v} \cdot \nabla U]_+] + O(\Delta t^2) \quad (\text{A.6})$$

where in (A.5) we did a Taylor expansion and in (A.6) we used (A.1).

The second term in (A.3) corresponds to being at  $(\mathbf{w} - \mathbf{v}_r\Delta t, \mathbf{v}_r)$  at time  $t$ , moving  $\mathbf{v}_r\Delta t$  and bouncing. This occurs with probability  $\Delta t[\mathbf{v}_r \cdot \nabla U]_+ = \Delta t[-\mathbf{v} \cdot \nabla U]_+$ , so we have

$$[p_{t+\Delta t}(\mathbf{w}, \mathbf{v})]_r = \Delta t[-\mathbf{v} \cdot \nabla U]_+p_t(\mathbf{w} - \mathbf{v}_r\Delta t, \mathbf{v}_r) \quad (\text{A.7})$$

$$= \Delta t[-\mathbf{v} \cdot \nabla U]_+p_t(\mathbf{w}, \mathbf{v}_r) + O(\Delta t^2) \quad (\text{A.8})$$

where again we did a Taylor expansion in (A.7). Adding (A.6) and (A.8), and using

$$[\mathbf{v} \cdot \nabla U]_+ - [-\mathbf{v} \cdot \nabla U]_+ = \mathbf{v} \cdot \nabla U, \quad (\text{A.9})$$

equation (A.3) becomes

$$p_{t+\Delta t}(\mathbf{w}, \mathbf{v}) = p_t(\mathbf{w}, \mathbf{v}) + O(\Delta t^2), \quad (\text{A.10})$$

which implies that the distribution is stationary,  $\frac{dp_t(\mathbf{w}, \mathbf{v})}{dt} = 0$ .

## A.2 Noisy Gradient

Consider now a noisy gradient represented as

$$\nabla \tilde{U}(\mathbf{w}) = \nabla U(\mathbf{w}) + \mathbf{n}_w, \quad \mathbf{n}_w \sim p(\mathbf{n}_w|\mathbf{w}), \quad \mathbf{n}_w \in \mathbb{R}^D \quad (\text{A.11})$$

where we assume that  $p(\mathbf{n}_w|\mathbf{w})$  has zero mean.

First note that the requirement that  $\mathbf{n}_w$  and  $\mathbf{n}'_w$  are conditionally independent given  $\mathbf{w}$  and  $\mathbf{w}'$ , with  $\mathbf{w} \neq \mathbf{w}'$ , is needed to preserve under the noise the Markov property of the sampler, which requires the bounce point process intensity to depend only on  $\mathbf{w}$ , and not the past history of the  $\mathbf{w}$  trajectory.

Next we decompose the random vector  $\mathbf{n}_w$  into a component along  $\mathbf{v}$ , given by  $y = \mathbf{v} \cdot \mathbf{n}_w$ , and an orthogonal component  $\mathbf{n}_v$ , satisfying  $\mathbf{n}_v \cdot \mathbf{v} = 0$ . This induces a corresponding decomposition in the probability density as

$$d\mathbf{n}_w p(\mathbf{n}_w|\mathbf{w}) = dy d\mathbf{n}_v p(y|\mathbf{w}) p(\mathbf{n}_v|y, \mathbf{w}, \mathbf{v}), \quad (\text{A.12})$$

and note that from the assumption that  $p(\mathbf{n}_w|\mathbf{w})$  has zero mean it follows that  $p(y|\mathbf{w})$  has zero mean. The noisy projected gradient becomes

$$\tilde{G}(\mathbf{w}) = \mathbf{v} \cdot \nabla U(\mathbf{w}) + y, \quad y \sim p(y|\mathbf{w}). \quad (\text{A.13})$$

To study the invariance of  $p(\mathbf{w}, \mathbf{v})$  under the noisy BPS, let us consider again the decomposition (A.3) into straight and bounced infinitesimal trajectories. The probability that the particle is at  $(\mathbf{w} - \mathbf{v}\Delta t, \mathbf{v})$  at time  $t$  and moves a distance  $\mathbf{v}\Delta t$  without bouncing is the average of  $1 - \Delta t[\tilde{G}]_+$  over all the possible realizations of  $y$ , and is therefore given by

$$1 - \Delta t P_v \equiv 1 - \Delta t \int_{-\infty}^{+\infty} [\mathbf{v} \cdot \nabla U(\mathbf{w}) + y]_+ p(y|\mathbf{w}) dy \quad (\text{A.14})$$

$$= 1 - \Delta t \int_{-\mathbf{v} \cdot \nabla U(\mathbf{w})}^{+\infty} (\mathbf{v} \cdot \nabla U(\mathbf{w}) + y) p(y|\mathbf{w}) dy \quad (\text{A.15})$$

The first term of (A.3) is therefore

$$[p_{t+\Delta t}(\mathbf{w}, \mathbf{v})]_d = (1 - \Delta t P_v) p(\mathbf{w} - \mathbf{v}\Delta t, \mathbf{v}) \quad (\text{A.16})$$

$$= p_t(\mathbf{w}, \mathbf{v}) - \Delta t \mathbf{v} \cdot \nabla p_t(\mathbf{w}) p_t(\mathbf{v}) - \Delta t P_v p_t(\mathbf{w}) p_t(\mathbf{v}) + O(\Delta t^2) \quad (\text{A.17})$$

similarly to (A.4)-(A.6).

The second term in (A.3) now has contributions from all those values  $(\mathbf{w} - \tilde{\mathbf{v}}_r \Delta t, \tilde{\mathbf{v}}_r)$  at time  $t$ , such that a reflection of  $\tilde{\mathbf{v}}_r$  with respect to a noisy  $\nabla \tilde{U}(\mathbf{w})$  gives  $\mathbf{v}$ . Such a  $\tilde{\mathbf{v}}_r$  exists for every value of the noise vector  $\mathbf{n}_w$ , and is given by

$$\tilde{\mathbf{v}}_r = \mathbf{v} - 2 \frac{(\mathbf{v} \cdot \nabla \tilde{U}(\mathbf{w})) \nabla \tilde{U}(\mathbf{w})}{\|\nabla \tilde{U}(\mathbf{w})\|^2} \quad (\text{A.18})$$

Therefore the second term in (A.3) contains contributions from all the possible realizations of  $\mathbf{n}_w$  and is

$$[p_{t+\Delta t}(\mathbf{w}, \mathbf{v})]_r = \Delta t \int_{\mathbb{R}^D} d\mathbf{n}_w [\tilde{\mathbf{v}}_r \cdot \nabla \tilde{U}(\mathbf{w})]_+ p(\mathbf{n}_w|\mathbf{w}) p_t(\mathbf{w} - \tilde{\mathbf{v}}_r \Delta t, \tilde{\mathbf{v}}_r) \quad (\text{A.19})$$

$$= \Delta t p_t(\mathbf{w}, \tilde{\mathbf{v}}_r) \int_{-\infty}^{+\infty} dy p(y|\mathbf{w}) [-\mathbf{v} \cdot \nabla U(\mathbf{w}) - y]_+ \times \int d\mathbf{n}_v p(\mathbf{n}_v|y, \mathbf{w}, \mathbf{v}) + O(\Delta t^2) \quad (\text{A.20})$$

where we used  $\tilde{\mathbf{v}}_r \cdot \nabla \tilde{U}(\mathbf{w}) = -\mathbf{v} \cdot \nabla U(\mathbf{w}) - y$ , the measure decomposition (A.12),  $\int d\mathbf{n}_v p(\mathbf{n}_v|y, \mathbf{w}, \mathbf{v}) = 1$  and defined

$$P_{\mathbf{v}_r} = \int_{-\infty}^{-\mathbf{v} \cdot \nabla U(\mathbf{w})} dy (-\mathbf{v} \cdot \nabla U(\mathbf{w}) - y) p(y|\mathbf{w}). \quad (\text{A.21})$$

Adding now (A.17) and (A.20), using  $p(\tilde{\mathbf{v}}_r) = p(\mathbf{v})$  (since  $p(\mathbf{v})$  is uniform) and

$$P_{\mathbf{v}} - P_{\mathbf{v}_r} = \mathbf{v} \cdot \nabla U(\mathbf{w}), \quad (\text{A.22})$$

which follows from (A.15) and (A.21), and the fact that  $p(y|\mathbf{w})$  has zero mean, we get again the stationarity condition

$$p_{t+\Delta t}(\mathbf{w}, \mathbf{v}) = p_t(\mathbf{w}, \mathbf{v}) + O(\Delta t^2). \quad (\text{A.23})$$

## B SBPS algorithm

Algorithm 2 provides a description of the SBPS algorithm with a linear regression based thinning proposal intensity. We have omitted velocity refreshments for the sake of clarity.  $\Delta t$  in the code below is the resolution of the piecewise linear proposal intensity, which should be smaller than the typical time between bounces. In all experiments a value of  $\Delta t = .01$  was used.

---

### Algorithm 2 Stochastic Bouncy Particle Sampler

---

#### SBPS:

Initialize particle position  $\mathbf{w} \in \mathbb{R}^D$ , velocity  $\mathbf{v} \in S^{D-1}$ ,  $t \leftarrow 0$ , regression coefficients  $\hat{\beta}_0, \hat{\beta}_1, \rho(t)$

**while** desired **do**

$t, \lambda(t) = \text{Sample\_Proposal\_Time}(\hat{\beta}_0, \hat{\beta}_1, \rho(t))$

$\mathbf{w} \leftarrow \mathbf{w} + \mathbf{v} * t$

    Store  $\mathbf{w}, t$

    Observe  $\nabla \tilde{U}(\mathbf{w})$ ,  $\text{Var}[\mathbf{v} \cdot \nabla \log p(x_{r_i}|\mathbf{w})]$

    (optional: Update preconditioner and apply it to gradient - see C)

    Calculate  $\tilde{G}(t), c(t)$

$\mathbf{v} = \text{Accept/Reject\_Proposal}(\tilde{G}(t), \lambda(t), \mathbf{v})$

$\hat{\beta}_0, \hat{\beta}_1, \rho(t) = \text{Update\_Local\_Regression\_Coefficients}(\tilde{G}(t), c(t), t)$

**end while**

**return** Return piecewise linear trajectory of  $\mathbf{w}$

#### Sample \_ Proposal \_ Time( $\hat{\beta}_0, \hat{\beta}_1, \rho(t)$ ):

$t_{\text{next\_proposal}} \leftarrow 0$

    Initialize set of interpolation points  $p = \{[\hat{\beta}_1 t_{\text{next\_proposal}} + \hat{\beta}_0 + k\rho(t_{\text{next\_proposal}})]_+\}$

    Initialize piecewise linear proposal intensity  $\lambda(t) = \text{Inter}(p)^*$

    Draw  $u \sim \mathcal{U}[0, 1]$

**while**  $-\log(u) > \int_0^{t_{\text{next\_proposal}}} \lambda(t) dt$  **do**

$t_{\text{next\_proposal}} \leftarrow t_{\text{next\_proposal}} + \min(\Delta t, -\log(u) - \int_0^{t_{\text{next\_proposal}}} \lambda(t) dt)$

$p \leftarrow p \cup [\hat{\beta}_1 t_{\text{next\_proposal}} + \hat{\beta}_0 + k\rho(t_{\text{next\_proposal}})]_+$

$\lambda = \text{Inter}(p)$

**end while**

    Return  $t_{\text{next\_proposal}}, \lambda(t_{\text{next\_proposal}})$

\*  $\text{Inter}(p)$  is a linear interpolation of the points in  $p$  and their respective times since the last proposal

---

---

**Accept/Reject – Proposal**( $\tilde{G}(t), \lambda(t), \mathbf{v}$ ):

Draw  $u \sim \mathcal{U}[0, 1]$

**if**  $u > \tilde{G}(\mathbf{w})/\lambda(t)$  **then**

    Proposed bounce time accepted:

    Initialize  $\{\tilde{G}(t_i), c(t_i)\}$  and regression coefficients  $\hat{\beta}_0, \hat{\beta}_1, \rho(t)$  using  $\tilde{G}(t), c(t)$

    Return  $\mathbf{v} - 2 \frac{(\mathbf{v} \cdot \nabla \tilde{U}(\mathbf{w})) \nabla \tilde{U}(\mathbf{w})}{\|\nabla \tilde{U}(\mathbf{w})\|^2}$

**else**

    Proposed bounce time rejected, maintain current trajectory:

    Return  $\mathbf{v}$

**end if**

---

**Update – Local – Regression – Coefficients**( $\tilde{G}(t), c(t), t$ ):

Add  $\tilde{G}(t), c(t)$  to  $\{\tilde{G}(t_i), c(t_i)\}$

(optional: Perform hyperparameter learning step on regression priors)

Update regression coefficients  $\hat{\beta}_0, \hat{\beta}_1, \rho(t')$  using standard Bayesian regression formula

(optional: If  $\hat{\beta}_1 < 0$  set  $\hat{\beta}_1$  to non-negative value, update  $\hat{\beta}_0$  accordingly)

Return  $\hat{\beta}_0, \hat{\beta}_1, \rho(t)$

---

## C Preconditioned SBPS

Consider now the linear transformation

$$\mathbf{w} = \mathbf{A}\mathbf{z} \quad (\text{C.24})$$

with an arbitrary square matrix  $\mathbf{A}$ . A distribution  $p(\mathbf{w})$  of interest can be expressed in terms of  $\mathbf{z}$  as

$$p_z(\mathbf{z})d\mathbf{z} = p(\mathbf{w}(\mathbf{z}))d\mathbf{w} = p(\mathbf{A}\mathbf{z})|\mathbf{A}|d\mathbf{z}, \quad (\text{C.25})$$

$$= \exp(-U_z(\mathbf{z}))d\mathbf{z}. \quad (\text{C.26})$$

The SBPS algorithm can be applied to the density  $p_z(\mathbf{z})$  using the gradients of  $U(\mathbf{w})$ . For this note that

$$\nabla_z U_z(\mathbf{z}) = \mathbf{A} \nabla_w U(\mathbf{w}). \quad (\text{C.27})$$

The Poisson intensity to compute bounces is  $[G]_+$ , with  $G = \mathbf{v} \cdot \mathbf{A} \nabla U(\mathbf{w})$ , and the velocity reflection is computed as

$$\mathbf{v}_r = \mathbf{v} - 2 \frac{(\mathbf{v} \cdot \mathbf{A} \nabla U(\mathbf{w})) \mathbf{A} \nabla U(\mathbf{w})}{\|\mathbf{A} \nabla U(\mathbf{w})\|^2}. \quad (\text{C.28})$$

Note also from (C.24) that the piecewise linear trajectory  $\mathbf{z}_t = \mathbf{z}_0 + \mathbf{v}t$  becomes

$$\mathbf{w}_t = \mathbf{w}_0 + \mathbf{A}\mathbf{v}t \quad (\text{C.29})$$

The matrix  $\mathbf{A}$  is called a preconditioner in the optimization literature, but can also be used in a sampling context to reduce anisotropy of posterior distributions; it is often the case that a good preconditioner is not known in advance but is instead learned adaptively [29].

We use a diagonal preconditioner for simplicity. Denoting the  $i$ th component at the  $j$ th evaluation of the gradient by  $g_i^j$ , we define

$$a_i^j = \beta(g_i^j)^2 + (1 - \beta)a_i^{j-1}, \quad (\text{C.30})$$

$$\tilde{a}^j = \frac{1}{d} \sum_{i=1}^d \frac{1}{\sqrt{a_i^j} + \epsilon} \quad (\text{C.31})$$

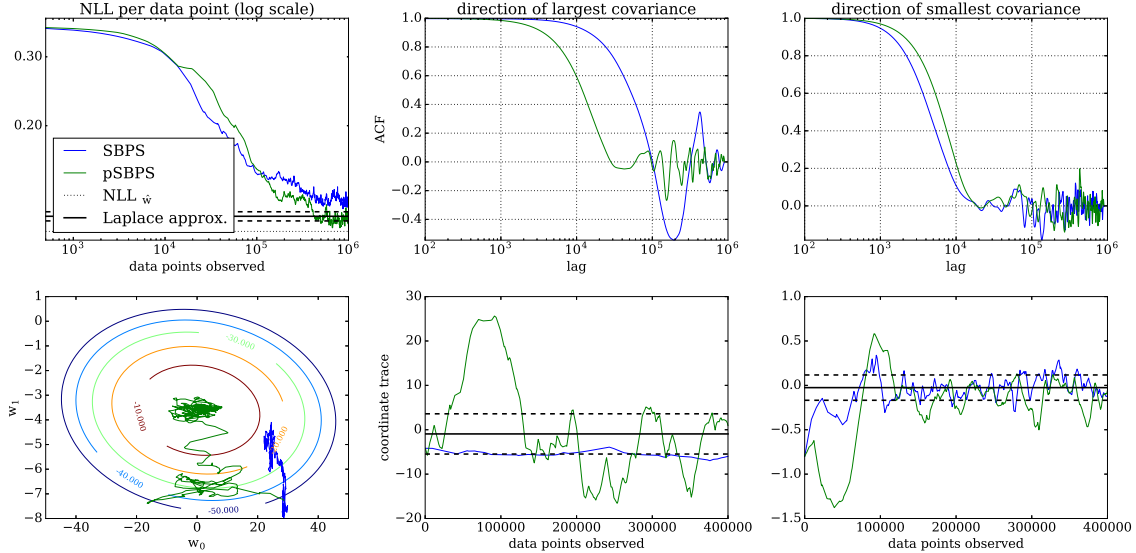


Figure 6: Effect of diagonal preconditioning on SBPS performance. Sampling is from the logistic regression posterior as described in section 6.1, with  $d = 20, N = 1000, k = 3, n = 100$ . The preconditioner parameters are  $\beta = .99, \epsilon = 10^{-4}$ . *Top Left:* NLL per data point for samples of SBPS and pSBPS. *Bottom Left:* Projection of the SBPS and pSBPS trajectories onto two dimensions. The contour plots are the posterior log likelihood under the Laplace approximation. *Center, Right:* ACF and trajectories in the direction of least and greatest covariance.

for some  $0 \leq \beta \leq 1, \epsilon \ll 1$ . The preconditioner at iteration  $j$  is defined as

$$\mathbf{A}^j = \text{Diag} \left( \frac{\tilde{a}^j}{\sqrt{a_i^j + \epsilon}} \right) \quad (\text{C.32})$$

This is the same preconditioner used in [30], up to the  $\tilde{a}^j$  factor; the latter is needed here in order to prevent scaling of  $\tilde{G}$ .

As noted in [30], a time dependent preconditioner requires adding a term proportional to  $\frac{\partial \mathbf{A}^j}{\partial \mathbf{w}}$  to the preconditioned gradient, yet this term is negligibly small and can be ignored when  $\beta \approx 1$ , since in this parameter regime the preconditioner changes slowly as a function of  $j$  and thus of  $\mathbf{w}$ .

We call this preconditioned variant pSBPS. It performs favorably compared to SBPS in cases where the posterior is anisotropic and axis-aligned, since we use a diagonal approximation of the Hessian in the preconditioner. As Figure 6 shows, pSBPS converges to the posterior mode faster than SBPS, and exhibits faster mixing in the direction of greatest covariance.

## D SGLD Step Size Scan

In the logistic regression example of Section 6.1, we compare SBPS with Stochastic Gradient Langevin Dynamics (SGLD) [4] with fixed step size. A natural question is how to choose an appropriate step size that ensures the fastest possible mixing without introducing an unacceptable amount of bias. Our criterion was to pick the biggest possible (i.e., fastest-mixing) step size such that the resulting variance of the per-data-point Negative Log Likelihood (NLL) coincides with that of the Laplace approximation. The latter gives a per-data-point NLL distribution of  $\frac{1}{2N} \chi^2(d) + NLL_{\hat{w}}/N$  where  $\hat{w}$  is the MAP estimator [31]. The results of this parameter scan are shown in Figure 7 and suggest a step size of 0.1.

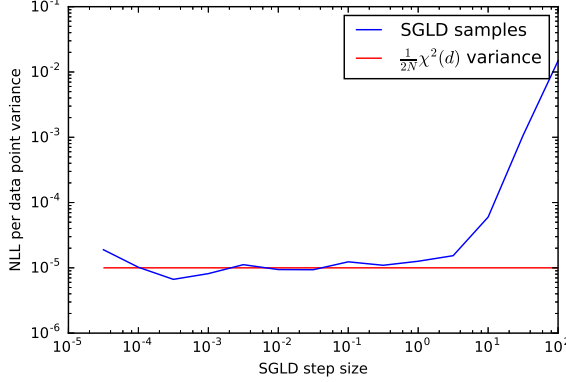


Figure 7: Per-data-point variance of the NLL in the logistic regression example of Section 6.1, using SGLD samples with step sizes of  $10^{-i/2}$ ,  $i = 0 \dots 9$ . The samplers were initialized at the MAP. We select the biggest step size whose empirical variance is below that from the Laplace approximation,  $\frac{d}{2N^2}$ .

## E The effect of the SBPS hyperparameters

In this section we explore, in the logistic regression example of Section 6.1, the effect of two hyperparameters that control the behavior of SBPS: the mini-batch size  $n$ , and the width  $k$  of the upper confidence band. A third hyperparameter is the rate of velocity refreshments, shown in [13] to be necessary in general to prove ergodicity. But, as mentioned in Section 4, in the examples we considered the mini-batch noise was enough to sufficiently randomize possible non-mixing trajectories, so we could safely set this parameter to a very low value.

### E.1 Mini-batch size $n$

Figure 8 shows an exploration of different values of the mini-batch size  $n$ . Low values for  $n$  lead to high noise for  $\tilde{G}$ . This in turn yields higher values for the proposal intensity  $\gamma(t)$ , which leads to shorter linear trajectories between bounce proposals. This is consistent with the results of Figure 8 that show a linear relation between  $n$  (i.e. computational cost per bounce proposal) and the average travel time between bounces. The autocorrelation functions (ACFs) were computed from discrete samples obtained by running SBPS with different  $n$ 's such that the total data cost was the same for all cases, and then discretizing the continuous paths into equal numbers of uniformly spaced samples. As shown, these cost adjusted ACFs are quite similar. On the other hand, the upper-left panel, shows that lower values of  $n$  have faster convergence to equilibrium, suggesting that low  $n$  should be preferred. But this should be contrasted with the fact that shorter linear trajectories increase the variance of expectations over rapidly changing functions, as discussed in Section 6.3.

### E.2 Upper-band width $k$

Figure 9 shows an exploration of different values of  $k$ , the height of the proposal intensity above the estimator mean, in units of predictive standard deviation (see in Eq.(16)). It therefore controls the trade-off between a regime, at low  $k$ , of faster mixing and high bias from violations of the thinning upper bound ( $[\tilde{G}(t)]_+/\lambda(t) > 1$ ), and another regime, high  $k$ , of low bias and high variance from slower mixing. As expected, the rate of bound violation decreases monotonically with  $k$ , as seen in the bottom left panel of Figure 9.

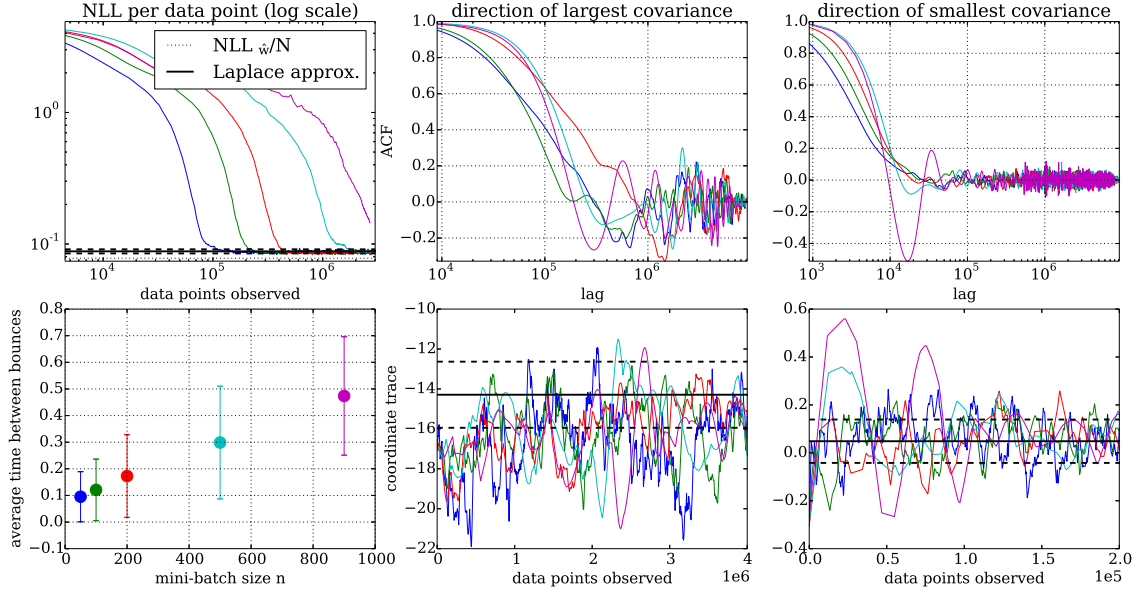


Figure 8: Effect of mini-batch sizes  $n$  in the logistic regression example of Section 6.1. Mini-batch sizes were 50, 100, 200, 500, 900. *Top Left*: Average per-data-point NLL over 5 runs. Note that smaller  $n$  lead to faster convergence to a region of low NLL. *Lower Left*: Estimated average time between particle bounces. *Center/Right*: ACF and trajectories from a single run, in the directions of smallest and biggest covariance. The x axis was chosen differently for the trajectory plots for clarity.

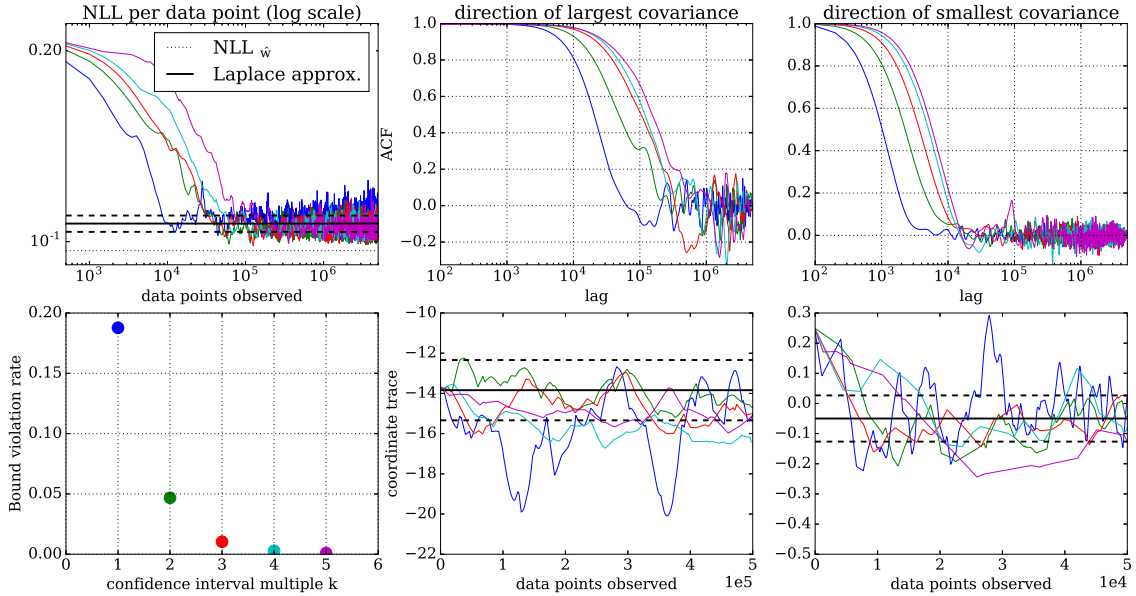


Figure 9: Effect of upper band size  $k$  in the logistic regression example of Section 6.1, run with mini-batch size  $n = 100$ . *Bottom Left*: Rate of upper bound violations as a function of  $k$ ; the same colors are used in the other plots. *Top Left*: NLL per data point for samples of SBPS with different  $k$  values. *Center/Right*: ACF and trajectories in the directions of smallest and biggest covariance. Note that smaller  $k$  leads to faster convergence and mixing but increased bias, as visible in the coordinate trace in the direction of biggest covariance. The x axis was chosen differently for the trajectory plots for clarity.

## F Upper Bound for Logistic Regression

In the case of logistic regression with data  $(y_i, \mathbf{x}_i)$  the estimator of  $\nabla_{\mathbf{w}}U(\mathbf{w})$  from a mini-batch of size  $n$  is

$$\nabla_{\mathbf{w}}\tilde{U}(\mathbf{w}) = \frac{N}{n} \sum_{i=1}^n \mathbf{x}_i (\sigma(\mathbf{w} \cdot \mathbf{x}_i) - y_i) \quad (\text{F.33})$$

A simple bound on  $\tilde{G}(t)$  is therefore given by

$$\tilde{G}(t) \leq \frac{N}{n} \left| \sum_{i=1}^n (\mathbf{v} \cdot \mathbf{x}_i) (\sigma(\mathbf{w} \cdot \mathbf{x}_i) - y_i) \right| \quad (\text{F.34})$$

$$\leq \frac{N}{n} \sum_{i=1}^n \|\mathbf{v}\|_2 \|(\sigma(\mathbf{w} \cdot \mathbf{x}_i) - y_i) \mathbf{x}_i\|_2 \quad (\text{F.35})$$

$$\leq \frac{N}{n} \sum_{i=1}^n \|x_i\|_2 \quad (\text{F.36})$$

$$\leq \sqrt{d}N \max_{i,j} |x_{ij}| \quad (\text{F.37})$$

Compared to the bound proposed in [13], this bound is more conservative but cheaper to compute and does not require non-negative covariates. It similarly scales like  $N$  and when the data used in the experiments was modified so that the covariates were non-negative the bounds differed by a factor lower than 2.

## Acknowledgements

We thank Alexandre Bouchard for correspondence. Funding for this research was provided by ONR N00014-14-1-0243 and a Google Faculty Research award; in addition, this work was supported by the Intelligence Advanced Research Projects Activity (IARPA) via Department of Interior/ Interior Business Center (DoI/IBC) contract number D16PC00003. The U.S. Government is authorized to reproduce and distribute reprints for Governmental purposes notwithstanding any copyright annotation thereon. Disclaimer: The views and conclusions contained herein are those of the authors and should not be interpreted as necessarily representing the official policies or endorsements, either expressed or implied, of IARPA, DoI/IBC, or the U.S. Government.

## References

- [1] Rémi Bardenet, Arnaud Doucet, and Chris Holmes. On Markov chain Monte Carlo methods for tall data. *arXiv:1505.02827*, 2015.
- [2] Anoop Korattikara, Yutian Chen, and Max Welling. Austerity in MCMC land: Cutting the Metropolis-Hastings budget. *arXiv:1304.5299*, 2013.
- [3] Rémi Bardenet, Arnaud Doucet, and Chris Holmes. Towards scaling up Markov chain Monte Carlo: an adaptive subsampling approach. In *ICML*, pages 405–413, 2014.
- [4] Max Welling and Yee W Teh. Bayesian learning via stochastic gradient Langevin dynamics. In *ICML*, pages 681–688, 2011.
- [5] Sam Patterson and Yee Whye Teh. Stochastic gradient Riemannian Langevin dynamics on the probability simplex. In *NIPS*, pages 3102–3110, 2013.
- [6] Tianqi Chen, Emily B Fox, and Carlos Guestrin. Stochastic gradient HMC. In *ICML*, pages 1683–1691, 2014.
- [7] Yi-An Ma, Tianqi Chen, and Emily Fox. A complete recipe for stochastic gradient MCMC. In *NIPS*, pages 2899–2907, 2015.
- [8] Sungjin Ahn, Anoop Korattikara, and Max Welling. Bayesian posterior sampling via stochastic gradient fisher scoring. *ICML*, 2012.
- [9] Nan Ding, Youhan Fang, Ryan Babbush, Changyou Chen, Robert D Skeel, and Hartmut Neven. Bayesian sampling using stochastic gradient thermostats. In *NIPS*, pages 3203–3211, 2014.
- [10] Dougal Maclaurin and Ryan P Adams. Firefly Monte Carlo: Exact MCMC with subsets of data. *arXiv:1403.5693*, 2014.
- [11] Matias Quiroz, Mattias Villani, and Robert Kohn. Exact Subsampling MCMC. *arXiv:1603.08232*, 2016.
- [12] EAJF Peters and G de With. Rejection-free Monte Carlo sampling for general potentials. *Phys. Rev. E*, 85(2):026703, 2012.
- [13] Alexandre Bouchard-Côté, Sebastian J Vollmer, and Arnaud Doucet. The Bouncy Particle Sampler: A Non-Reversible Rejection-Free Markov Chain Monte Carlo Method. *arXiv:1510.02451*, 2015.
- [14] Joris Bierkens and Gareth Roberts. A piecewise deterministic scaling limit of Lifted Metropolis-Hastings in the Curie-Weiss model. *arXiv:1509.00302*, 2015.
- [15] Joris Bierkens, Paul Fearnhead, and Gareth Roberts. The Zig-Zag Process and Super-Efficient Sampling for Bayesian Analysis of Big Data. *arXiv preprint arXiv:1607.03188*, 2016.

- [16] Radford M Neal. Improving asymptotic variance of MCMC estimators: Non-reversible chains are better. *arXiv preprint math/0407281*, 2004.
- [17] Marija Vucelja. Lifting–A Nonreversible MCMC Algorithm. *arXiv:1412.8762*, 2014.
- [18] Joris Bierkens and Andrew Duncan. Limit theorems for the zig-zag process. *arXiv preprint arXiv:1607.08845*, 2016.
- [19] Mark HA Davis. Piecewise-deterministic Markov processes: A general class of non-diffusion stochastic models. *J. Royal Stat. Soc., Series B (Methodological)*, pages 353–388, 1984.
- [20] David R Cox. Some statistical methods connected with series of events. *J. Royal Stat. Soc., Series B (Methodological)*, pages 129–164, 1955.
- [21] Jan Grandell. *Doubly stochastic Poisson processes*. Springer, 1976.
- [22] Peter A Lewis and Gerald S Shedler. Simulation of nonhomogeneous Poisson processes by thinning. *Naval Research Logistics Quarterly*, 26(3):403–413, 1979.
- [23] Christian Robert and George Casella. *Monte Carlo statistical methods*. Springer Science & Business Media, 2013.
- [24] Yi-An Ma, Tianqi Chen, Lei Wu, and Emily B Fox. A Unifying Framework for Devising Efficient and Irreversible MCMC Samplers. *arXiv preprint arXiv:1608.05973*, 2016.
- [25] Jackson Gorham and Lester Mackey. Measuring sample quality with stein’s method. In *Neural Information Processing Systems*, 2015.
- [26] Matias Quiroz, Mattias Villani, and Robert Kohn. Speeding up MCMC by efficient data subsampling. *Riksbank Research Paper Series*, (121), 2015.
- [27] Nicolas Chopin and James Ridgway. Leave Pima Indians alone: binary regression as a benchmark for Bayesian computation. *arXiv preprint arXiv:1506.08640*, 2015.
- [28] Chunyuan Li, Changyou Chen, Kai Fan, and Lawrence Carin. High-Order Stochastic Gradient Thermostats for Bayesian Learning of Deep Models. *arXiv preprint arXiv:1512.07662*, 2015.
- [29] John Duchi, Elad Hazan, and Yoram Singer. Adaptive subgradient methods for online learning and stochastic optimization. *Journal of Machine Learning Research*, 12(Jul):2121–2159, 2011.
- [30] Chunyuan Li, Changyou Chen, David Carlson, and Lawrence Carin. Preconditioned stochastic gradient langevin dynamics for deep neural networks. *AAAI*, 2016.
- [31] Peter J Bickel and Kjell A Doksum. *Mathematical Statistics: Basic Ideas and Selected Topics, volume I*, volume 117. CRC Press, 2015.